Supplemental Material to

Emergence of Topologically Non-trivial Spin-polarized States in a Segmented Linear Chain

Thang Pham[1,2,3,4,†], Sehoon Oh[1,2,†], Scott Stonemeyer[1,2,4,5], Brian Shevitski[1,2], Jeffrey D. Cain[1,2,4], Chengyu Song[6], Peter Ercius[6], Marvin L. Cohen[1,2], and Alex Zettl[1,2,4*]

[1]*Department of Physics, University of California at Berkeley, Berkeley, CA 94720, USA*

[2]*Materials Sciences Division, Lawrence Berkeley National Laboratory, Berkeley, CA 94720, USA*

[3]*Department of Materials Science and Engineering, University of California at Berkeley, Berkeley, CA 94720, USA*

[4]*Kavli Energy NanoSciences Institute at the University of California at Berkeley, Berkeley, CA 94720, USA*

[5]*Department of Chemistry, University of California at Berkeley, Berkeley, CA 94720, USA*

[6]*National Center for Electron Microscopy, The Molecular Foundry, One Cyclotron Road, Berkeley, CA 94720, USA*

†These authors contributed equally

*e-mail: azettl@berkeley.edu

Methods

***Materials synthesis*:** The synthesis procedure is similar to that previously reported for $HfTe_3$ [1]. In general, multiwalled carbon nanotubes (CNTs) (Cheap Tubes) are annealed in air at 515 °C for 20 minutes to open the end-caps before the filling step. The as-prepared CNTs (~1-4 mg) together with a stoichiometric amount of Hf powder and Te shot (~ 560 mg in total), and ~5 mg/cm^3 (ampoule volume) of iodine powder (transport agent) are sealed under high vacuum (10^{-6} torr) in a quarter-inch quartz ampoule. The sealed ampoule is kept at 520 °C for 7 days, and then either quenched or gradually cooled to room temperature (over 9 days). Control syntheses are also performed, in which the precursor powders contained either only one material (i.e., only Hf, Te, or I_2), or any combination of two reagents (e.g., only Hf and Te or only Hf and I_2). We find no evidence of a segmented chain structure within the CNTs in these control experiments.

***Materials characterization**:* The product is dispersed in isopropanol by a bath sonicator for 15 minutes, then drop-cast onto a copper grid for STEM investigation. The imaging and spectroscopy are carried out using TEAM 0.5 operating at 80 keV, with the probe convergent angle of 25 mrad and the probe current of 70 pA, at the National Center for Electron Microscopy (NCEM). The STEM simulation is implemented by using PRISM code developed by Dr. Ophus at NCEM (open-source software available online). The average-cell calculation is done by the template matching technique written in Python to increase the signal-to-noise ratio and quality of the STEM image.

Calculation methods: We use the generalized gradient approximation [2], norm-conserving pseudopotentials [3], and localized pseudo-atomic orbitals for the wavefunction expansion as implemented in the SIESTA code [4]. The spin-orbit interaction is considered using fully relativistic j-dependent pseudopotentials [5] in the l-dependent fully-separable nonlocal form using additional Kleinman-Bylander-type projectors [6,7]. We use 1×1×512 Monkhorst-Pack *k*-point mesh and 1000 Ry real-space mesh cut-off for all of our calculations. The van der Waals interaction is evaluated using the DFT-D2 correction [8]. Dipole corrections are included to reduce the fictitious interactions between chains generated by the periodic boundary condition in our supercell approach [9].

Atomic structure:

Supplemental Material Fig. S1 shows the atomic structure of the segmented chain Hf_2Te_9 obtained from DFT calculation. The atomic structure has mirror planes in the unit of Hf_2Te_9 denoted as M_y and M_z, perpendicular to *y*- and *z*-axis, respectively. The length of a block is 7.89 Å, and blocks are separated by 3.65 Å. Each block connects to each other, forming a linear chain as shown in Supplemental Material Fig. S1(a). Supplemental Material Figs. S1(b-d) show the basic building block of the structure, along the *x*-, *y*-, and *z*-axis, respectively. Each block has two Hf atoms and nine Te atoms, with sequence Te_3-Hf-Te_3-Hf-Te_3 along the chain (*z*) direction. Each Hf atom is surrounded by six Te atoms in a trigonal prismatic form. The adjacent Te atoms form isosceles triangles. The triangle at the center of the block is on the mirror plane perpendicular to the chain direction, while those on the sides of the block cant toward the center of the block.

We would like to note that single-chain transition-metal trichalcogenides (TMTs) materials prefer either trigonal prismatic or antiprismatic structures depending on the composition, similar to the way some transition-metal dichalcogenide (TMD) materials prefer the trigonal prismatic (1H) structure while others prefer the trigonal antiprismatic (1T or 1T') structure. Therefore, both of the trigonal prismatic and antiprismatic structures are included in the candidate structures. Energetically, the segmented chain prefers a trigonal prismatic structure, unlike the continuous single-chain $HfTe_3$, which prefers an antiprismatic structure[4]. The total energy of the segmented chain in the prismatic form is ~0.8 eV lower total energy per Hf_2Te_9 formula unit (f.u.) than the antiprismatic form.

Charge density:

Supplemental Material Fig. S2 shows the calculated charge density of the single-atomic segmented chain of Hf_2Te_9. The charge density between the blocks is very low and has minimum value at the middle point between the blocks, meaning that the blocks are vdW bonded, not covalently bonded. The real-space wavefunction of all the occupied states are also examined, $\psi_{nk}(r)$, showing no occupied states between the blocks, confirming the vdW bonding of the blocks.

Topological property:

We calculate the Zak phases of the n-th bands of the channel s, $\gamma_n^S = i\int_{-\pi/a}^{\pi/a} dk\, \langle u_{nk}^s|\partial_k|u_{nk}^s\rangle$, for all of the occupied states of the segmented chain isolated in vacuum by integrating the Berry connection, across the 1D Brillouin zone, where u^s_{nk} is the periodic part of the electron Bloch wave function with band index n and crystal momentum k of the channel s, and s = I, II are the time-reversal channels. Because of the presence of the time-reversal symmetry and the mirror symmetry with respect to M_z, $\gamma^s{}_n$ is quantized to 0 or π (mod 2π), corresponding to a topologically trivial or nontrivial band, respectively. Explicitly, We calculated $\gamma_n^S = Im\left[ln \prod_{i=1}^{N}\langle u_{nk_i}^s|u_{nk_i+1}^s\rangle\right]$ using the discretized k points, where Im […] is the imaginary part of […], k_i with i=1,…,N, k_{N+1}=k_1, and a periodic gauge, in which $u_{nk_{N+1}}^s(z) = u_{nk_1}^s(z)e^{-i2\pi z/a}$, is used.

We obtain the symmetry-protected topological Z_2 invariance by $(-1)^{Z_2} = e^{i\sum_n \gamma_n^I}$, where the sum is over the occupied bands only in channel I. That is, the Z_2 invariance is determined by the number of nontrivial occupied bands in one time-reversal channel. Specifically, odd and even numbers of nontrivial occupied bands mean Z_2 = 0 and 1, respectively. We obtain the Z_2 for the neutral case and for the hole-doped case, where two electrons per formula unit are subtracted in the DFT calculation, as shown in Supplemental Material Fig. S3. For the neutral case, Z_2 = 0, corresponding to a trivial insulator, while Z_2 = 1 for the h-doped case, corresponding to a topological mirror insulator. The calculated Zak phase of the highest occupied band is π. As the h-doped chain has two fewer electrons per unit cell than the neutral chain, the total Zak phase of the h-doped chain must differ from that of the neutral chain by π, owing to emptying of the highest occupied band, and provided the Hamiltonian of the h-doped system may be obtained adiabatically from the neutral system without closing the band gap.

Since the sum of the Zak phase over one channel is nothing more than the partial polarization of the channel, the Z_2 invariance can be obtained alternatively by $Z_2 = 2P^I/e = Q$ mod 2, where Q is the end charge of the finite-length chain and e is the electron charge. We make finite chains (~15 nm) for both neutral and the h-doped system. We define the end charge of a system as the net deviation of the charge

of the finite chain of the blocks on both edges from the average charge of the infinite length chain in two units. Explicitly, $Q = \rho_L + \rho_R - 2\overline{\rho}$, where ρ_L (ρ_R) is the charge of the finite chain in the block on the left (right) edge and $\overline{\rho}$ is the charge of infinite length chain in one unit. For neutral case, $Q = 0$, meaning trivial insulator while $Q = 3e$ for the h-doped case, meaning topological mirror insulator.

Hf_2Te_9 as a molecule:

We investigate the stability of an isolated Hf_2Te_9 molecule (one isolated block) using DFT calculation. We construct candidate structures of the isolated molecule both in vacuum and encapsulated inside CNT using the atomic positions of the segmented chain, and the atomic positions are relaxed by minimizing total energy. Supplemental Material Figs.4 and 5 show the obtained relaxed atomic structure of the isolated Hf_2Te_9 molecule in vacuum and in CNT, respectively. For both cases, the atomic structure of the molecule shows no significant change when it is isolated from the chain, except that the isosceles triangles of Te atoms on edges cant toward the center slightly more compared to the segmented chain configuration. We investigate possibilities for the molecule to change its shape to antiprismatic form, and to be separated to other small molecules and atoms. No additional possible atomic structure configurations which have lower energy than that of the structure shown in Supplemental Material Figs. 4 and 5 could be found.

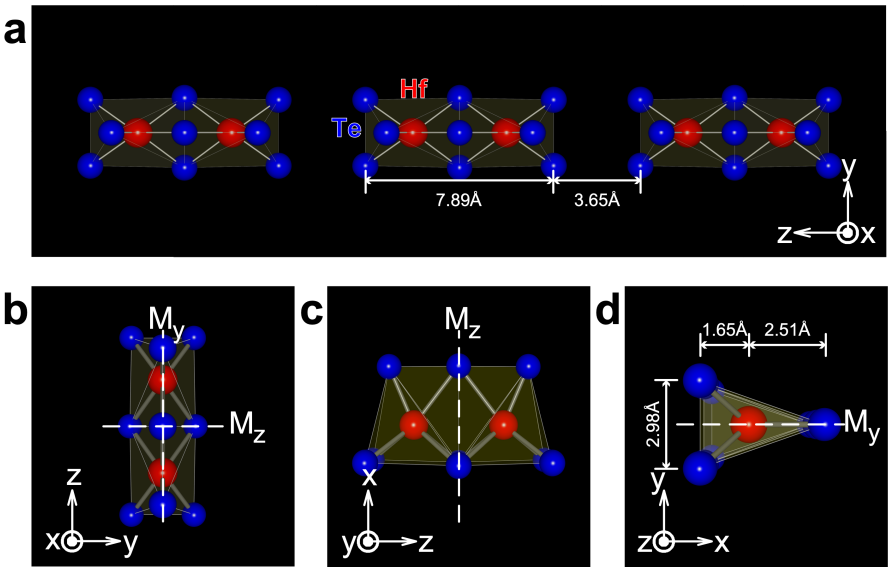

Supplemental Material Fig. S1. Atomic structure of the single-atomic segmented chain of Hf_2Te_9 obtained from DFT calculation. (a) The obtained atomic structure of the segmented single chain is shown, where Hf and Te atoms are represented as red and blue spheres, respectively, and chain direction is set to *z*-direction. (b-d) The atomic structure of the segmented chain of Hf_2Te_9 unit in side views along (b) *x*-axis and (c) *y*-axis, and (d) the axial view along *z*-axis, where the mirror planes in the unit perpendicular to *y*- and *z*-axes are represented by white dashed lines and denoted as M_y and M_z, respectively.

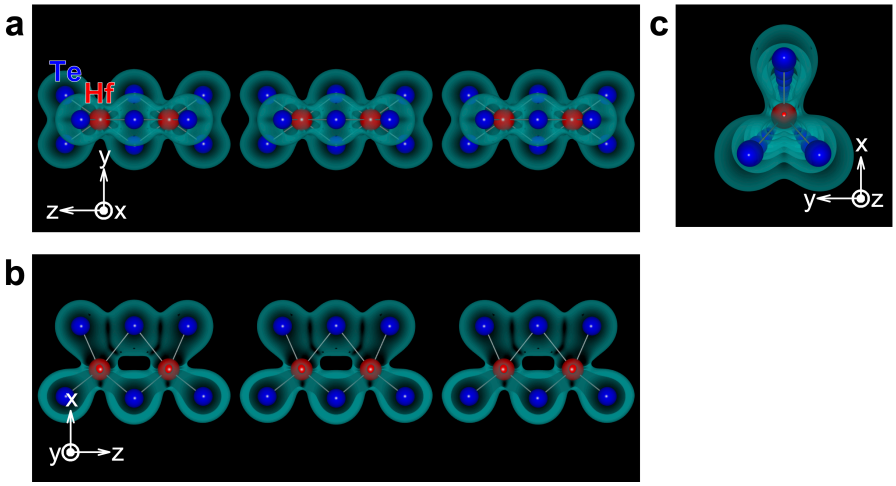

Supplemental Material Fig. S2. Charge density of the single-atomic segmented chain of Hf_2Te_9. Isosurface plots of the calculated charge density along with the atomic structures. Side views along (a) *x*-axis, (b) *y*-axis, and (c) axial view along *z*-axis. Hf and Te atoms are represented as red and blue spheres, respectively, and the isosurfaces are shaded in cyan.

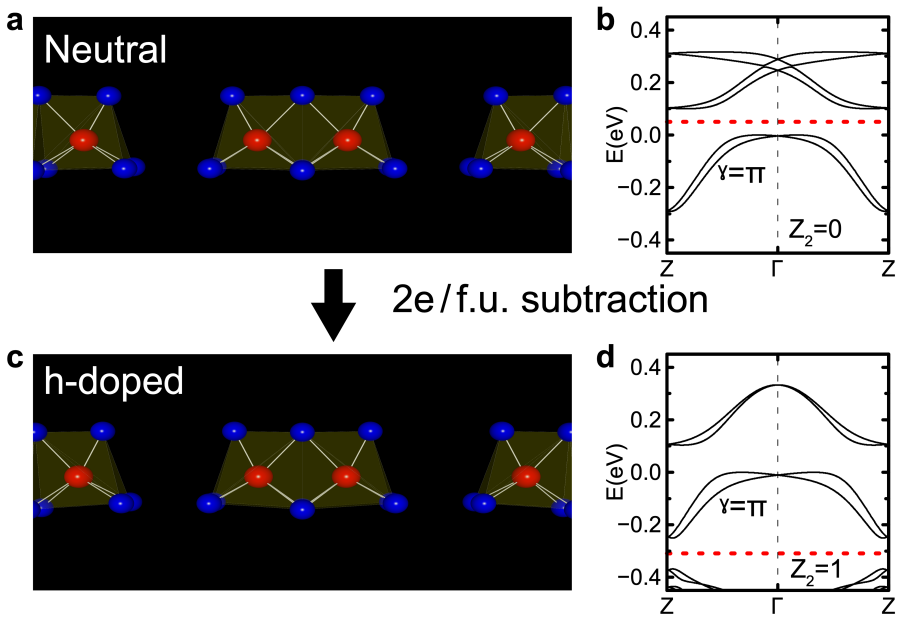

Supplemental Material Fig. S3. The single-atomic segmented chain of Hf_2Te_9 with chemical potential changed. (a, b) The atomic and electronic structure of the segmented chain of Hf_2Te_9 without chemical potential change (neutral) are shown for the comparison. (c, d) The atomic and electronic structure of the segmented chain of Hf_2Te_9 with two electron per formula unit subtracted in the DFT calculation (h-doped). In (a, c), Hf and Te atoms are represented as red and blue spheres, respectively. In (b, d), the energy level of the highest occupied band is set to zero, and the chemical potential is represented by red dashed line.

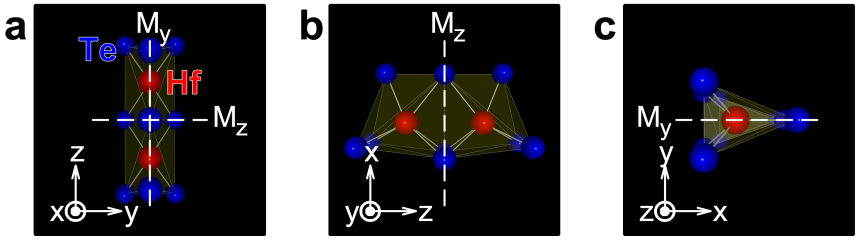

Supplemental Material Fig. S4. Hf_2Te_9 molecule isolated in vacuum. The atomic structure of the molecule is shown. Side views along (a) *x*-axis, (b) *y*-axis, and (c) axial view along *z*-axis. Hf and Te atoms are represented as red and blue spheres, respectively.

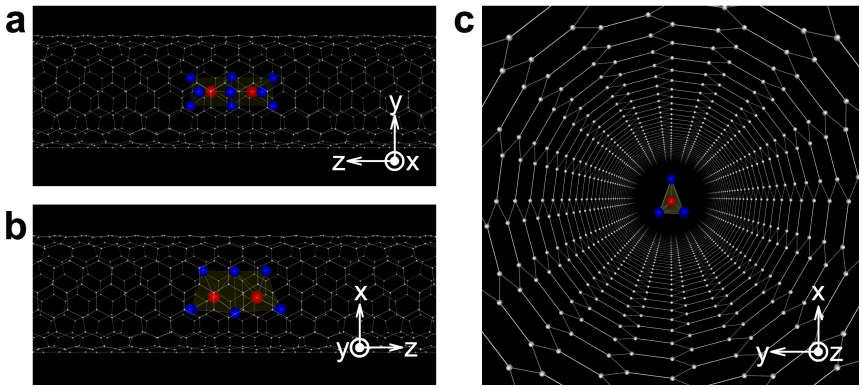

Supplemental Material Fig. S5. Hf_2Te_9 molecule encapsulated inside an (8,8) CNT. The atomic structure of the Hf_2Te_9 molecule encapsulated within the CNT is shown. Side views along (a) *x*-axis, (b) *y*-axis, and (c) axial view along *z*-axis, where Hf, Te and C atoms are represented as red, blue and white spheres, respectively.

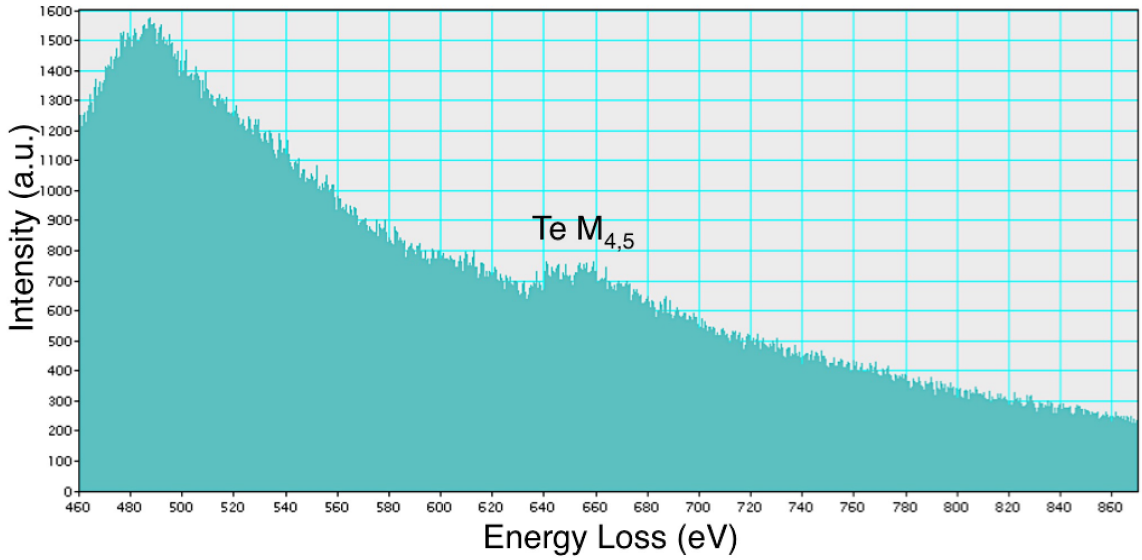

Supplemental Material Fig. S6. Electron Energy Loss (EEL) spectrum of Te M edges taken from a linear chain of Hf_2Te_9 blocks.

References

[1] Meyer, S. *et al.* Metal-insulator transition in quasi-one-dimensional $HfTe_3$ in the few-chain limit. *Phys. Rev. B* **100,** 041403 (2019)

[2] Perdew, J. P., Burke, K. & Ernzerhof, M. Generalized gradient approximation made simple. *Phys. Rev. Lett.* **77,** 3865–3868 (1996).

[3] Troullier, N. & Martins, J. L. Efficient pseudopotentials for plane-wave calculations. *Phys. Rev. B* **43,** 1993–2006 (1991).

[4] Soler, J. M. *et al.* The SIESTA method for ab initio order-N materials simulation. *Journal of Physics: Condensed Matter* **14,** 2745–2779 (2002).

[5] Kleinman, L. Relativistic norm-conserving pseudopotential. *Phys. Rev. B* **21,** 2630–2631 (1980).

[6] Theurich, G. & Hill, N. A. Self-consistent treatment of spin-orbit coupling in solids using relativistic fully separable *ab initio* pseudopotentials. *Phys. Rev. B* **64,** 073106 (2001).

[7] Kleinman, L. & Bylander, D. M. Efficacious form for model pseudopotentials. *Phys. Rev. Lett.* **48,** 1425–1428 (1982).

[8] Grimme, S. Semiempirical GGA type density functional constructed with a long-range dispersion correction. *Journal of Computational Chemistry* **27,** 1787–1799 (2006).

[9] Cohen, M. L., Schlüter, M., Chelikowsky, J. R. & Louie, S. G. Self-consistent pseudopotential method for localized configurations: Molecules. *Phys. Rev. B* **12,** 5575–5579 (1975).